

Update-Free On-Policy Steering via Verifiers

Maria Attarian^{1,2}, Ian Vyse³, Claas Voelcker⁴, Jasper Gerigk¹, Evgenii Opryshko¹, Anas Almasri¹, Sumeet Singh², Yilun Du⁵, Igor Gilitschenski¹

Abstract—In recent years, Behavior Cloning (BC) has become one of the most prevalent methods for enabling robots to mimic human demonstrations. However, despite their successes, BC policies are often brittle and struggle with precise manipulation. To overcome these issues, we propose UF-OPS, an Update-Free On-Policy Steering method that enables the robot to predict the success likelihood of its actions and adapt its strategy at execution time. We accomplish this by training verifier functions using policy rollout data obtained during an initial evaluation of the policy. These verifiers are subsequently used to steer the base policy toward actions with a higher likelihood of success. Our method improves the performance of black-box diffusion policy, without changing the base parameters, making it light-weight and flexible. We present results from both simulation and real-world data and achieve an average 49% improvement in success rate over the base policy across 5 real tasks.

I. INTRODUCTION

Behavior Cloning (BC) has become the de-facto standard for training manipulation policies from human teleop data [1–5]. Despite their popularity however, BC-based policies can be brittle with their performance varying wildly even within known tasks [6–8]. Failures of a BC policy often come from imprecise actions on crucial fine-grained interaction points [9–12]. A common strategy to mitigate these failures is to collect additional data around interaction points. However, this requires laborious and costly data collection and curation [10, 13], and human-collected data is not guaranteed to cover the policy’s actual failure modes [7, 14, 15].

To alleviate these issues, we use a rich source of data that is overlooked by other methods: the policy’s own evaluation. This data contains both successful demonstrations that could be used to reinforce what the policy does *right* and also failures that provide valuable information about what the policy does *wrong*. Intuitively, these failures contain crucial information about bottleneck states that require precise manipulation. We seek to develop a method that makes use of this failure data.

To leverage this data, we propose Update-Free On-Policy Steering (UF-OPS) which uses failed policy evaluations to *steer* the base BC policy [16, 17]. The core of UF-OPS is a trained verifier function, which predicts whether actions belong to a successful or failed rollout based on real evaluation data. This verifier function is then leveraged during further executions of the policy to nudge the action proposals of the base policies towards successful completion.

In contrast to prior works on using steering to guide robot policies [18–20], we focus on steering a policy using *its*

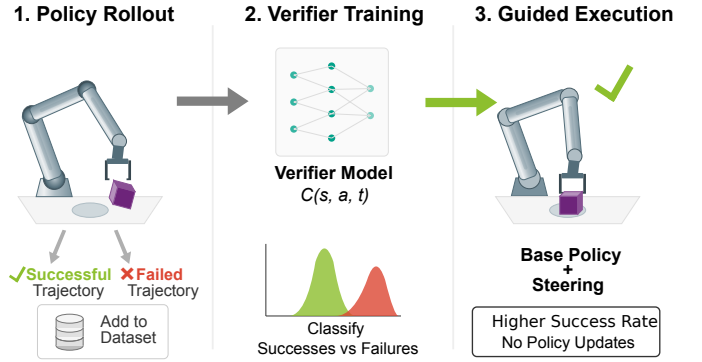


Fig. 1: Our method relies on a policy’s own evaluation data to improve its performance. Training small verifiers and subsequently, utilizing them via inference-time steering, allows for improved policy performance without costly data collections and resource extensive fine-tuning.

own experience i.e. trajectories collected by the policy itself, using both successful and failed trajectories. In addition, UF-OPS does not require finetuning the base policy, which means it is possible to apply it in compute-constrained, or black-box scenarios, and it mitigates the risk of catastrophic forgetting [21]. Finally, UF-OPS is fast and sample efficient in training and inference.

We show that using a policy’s own failures leads to efficient steering, even with limited interactions. In simulated manipulation tasks in the robomimic task suite [6], we find that UF-OPS is able to improve upon a base diffusion policy more reliably and with significantly smaller costs than prior methods. In five real bi-arm manipulation tasks on the Aloha system, we find that UF-OPS leads to increased success improvements of 25 to 80 percentage points, a substantial improvement over the base diffusion policies. It is able to achieve this with as little as a hundred evaluation trajectories per task.

II. RELATED WORK

Our work falls within the general area of adapting a pre-trained policy to improve its performance on a selection of robotic tasks. In general, three broad strategies have emerged to accomplish policy improvement. First, additional demonstration data can be gathered for further refinement of the policy using imitation or reinforcement learning (Sec. II-A). Second, careful manual or automatic curation of the datasets used for imitation learning can be used to improve base policy training, either via pre-training from scratch or through fine-tuning (Sec. II-B). The final approach is to directly steer

¹ University of Toronto; ²Google DeepMind; ³University of Alberta;

⁴UTAustin; ⁵Harvard University

Corresponding author: Maria Attarian.

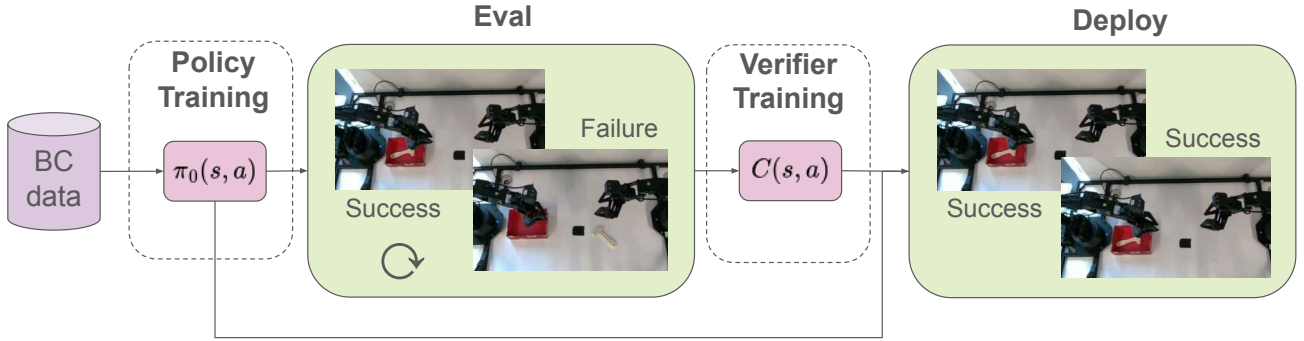


Fig. 2: Method overview: Given a base policy trained on a dataset of expert demonstrations, policy evaluation provides successful and failed rollouts. These are used for training a *verifier function* that scores a transition (s, a) in terms of its success likelihood. Finally, the verifier function is used in combination with a steering strategy, to improve the policy performance.

the policy without modifying its weights. We briefly survey important works in these areas to discuss advantages and disadvantages compared to our method (Sec. II-C).

A. Fine-tuning for Self-improvement

Policy improvement via obtaining new data and fine-tuning is a well-established field [7, 22–24]. The seminal method for improving imitation learning based on policy rollouts is DAgger [7] where successful policy rollouts are included for fine-tuning in a continual learning fashion. A more recent notable work is RoboCat [22] where authors presented an iterative self-improvement loop, where a specialized fine-tuned agent is deployed to generate thousands of successful self-collected trajectories for a new task, which are then added back to the master dataset to train a more capable generalist agent in the next iteration.

Another popular method for fine-tuning is reinforcement learning. While reinforcement learning has classically focused on training the whole policy from scratch, some recent works have shifted their attention to finetuning [25–28]. Our work is closest to Raad et al. [28] where an optimality predictor or success classifier is trained to predict the probability of task success given a state-action pair which is subsequently used as a reward model for RL fine-tuning of a previously fine-tuned VLM on robot trajectories. Unlike this, we refrain from updating the weights of the base policy.

B. Data Curation

Another line of work within self-improvement looks into the problem of data quality and proposes ways to collect higher quality data for training better policies. Notable works are SEIL [29] where expert trajectories are augmented with new simulated transitions alongside with an equivariant model exploiting symmetries in $SO(2)$, SART [30] which leverages a single demonstration with precision-boundary annotations followed by robot self-augmentation within these boundaries, and finally Demo-SCORE [31] which trains a classifier on success and failure rollouts and subsequently uses that to filter the base dataset for robust strategies resulting in a better performing retrained policy. Our work is closest to the last with our main difference being that we do not retrain the base policy

but instead directly guide it to choose higher value actions at test time.

C. Steering and Guidance for Policy Improvement

Finally, steering or guiding a pretrained base model towards policy improvement has gained traction recently [17, 19, 32–36]. DSRL [36] proposes diffusion steering via performing RL on the latent-noise space. This is done by using RL to train a policy which produces the noise samples used by the main BC diffusion policy. CFGRL [33] trains a diffusion policy with Classifier-Free Guidance using the advantage function. DynaGuide [18] trains a goal-conditioned dynamics model for classifier guidance. Our work is closest to V-GPS [35] where the authors propose steering via a Q function trained on a large general purpose dataset with offline RL, in order to improve base VLA performance. Unlike V-GPS, we focus on *self-improvement* and use targeted, relatively small datasets easily obtained from the policy itself without the requirement for human teleoperation. This allows us to sidestep the brittle and hard-to-tune pessimism parameter that is inherent to offline RL methods such as offline Q learning.

III. BACKGROUND: DIFFUSION POLICIES

Behavioral Cloning [37] is trained to reproduce the actions for each observation in a demonstration dataset, which is commonly assumed to contain only relevant and helpful actions to complete a task. Within this setup, a state-of-the-art approach is to represent the policy with a diffusion model [3]. Diffusion models were first developed for image generation, where they delivered impressive high-fidelity results [38–40]. They were later adapted to the imitation learning setting as *Diffusion Policies* [3] and have since become the de facto best design choice for manipulation systems.

The goal of diffusion models is to sample from a target distribution $q(x_0)$. In order to do so, this distribution is approximated by a parameterized distribution $p_\theta(x_0) = \int p_\theta(x_{0:T}) dx_{1:T}$. The sequence of distributions continually interpolates between a simple reference distribution, often a standard normal, and the target. For this work, we rely on the standard DDPM method [39], for which we provide the equations here. In this variant, β_t represents the timestep



Fig. 3: Real tasks on the Aloha bimanual system [12]. From left to right, a) pick up the block and place it on the cardboard, b) pick up the ball and place it in the bowl, c) pick up the hammer with the right hand, hand it over to the left hand and drop it in the box, d) pick up the pen cap with the right hand and the cap with the left and insert it on the pen, and e) pick up the green cup and stack it on the purple.

dependent level of noise added in the forward process:

$$q(\mathbf{x}_{1:T}|\mathbf{x}_0) = \prod_{t=1}^T q(\mathbf{x}_t|\mathbf{x}_{t-1}), \quad (1)$$

$$q(\mathbf{x}_t|\mathbf{x}_{t-1}) := \mathcal{N}(\mathbf{x}_t; \sqrt{1 - \beta_t}\mathbf{x}_{t-1}, \beta_t\mathbf{I}).$$

The model is then trained to predict the added noise. Finally, the clean sample is generated via the reverse diffusion process:

$$p_\theta(\mathbf{x}_{0:T}) = p(\mathbf{x}_T) \prod_{t=1}^T p_\theta(\mathbf{x}_{t-1}|\mathbf{x}_t), \quad (2)$$

$$p_\theta(\mathbf{x}_{t-1}|\mathbf{x}_t) := \mathcal{N}(\mathbf{x}_{t-1}; \boldsymbol{\mu}_\theta(\mathbf{x}_t, t), \boldsymbol{\Sigma}_\theta(\mathbf{x}_t, t))$$

Given a learned model $\epsilon_\theta(\mathbf{x}_t)$, the reverse process for DDPM simplifies to:

$$\mathbf{x}_{t-1} = \frac{1}{\sqrt{\alpha_t}} \left(\mathbf{x}_t - \frac{1 - \alpha_t}{\sqrt{1 - \alpha_t}} \epsilon_\theta(\mathbf{x}_t, t) \right) + \sigma_t \mathbf{z} \quad (3)$$

for each $t \in (T, \dots, 1)$, where $\alpha_t = 1 - \beta_t$, $\bar{\alpha}_t = \prod_{s=1}^t \alpha_s = \prod_{s=1}^t (1 - \beta_s)$ and $\beta_t \in (0, 1)$ is the variance schedule.

To adapt diffusion models to the behavior cloning setting, the model is expanded by an additional conditional input, the state observation \mathbf{s} . The diffused sample corresponds to the action that the robot is executing. In addition, it has become common practice to generate a small sequence of n actions in one go, a strategy commonly known as action chunking [12]. For a sequence of actions $\mathbf{a}^{[1:n]}$, the diffusion process becomes

$$\mathbf{a}_{t-1}^{[1:n]} = \frac{1}{\sqrt{\alpha_t}} \left(\mathbf{a}_t^{[1:n]} - \frac{1 - \alpha_t}{\sqrt{1 - \alpha_t}} \epsilon_\theta(\mathbf{a}_t^{[1:n]}, t | \mathbf{s}) \right) + \sigma_t \mathbf{z} \quad (4)$$

IV. POLICY STEERING WITH EVALUATION ROLLOUTS

While diffusion policies have shown great promise and impressive results, they continue to be data hungry [4]. Further, as mentioned, when these policies are evaluated, large amounts of *on-policy data* is generated, yet this additional, low cost source of data is underutilized, especially in real robotics settings, despite containing information on the policies specific *failure* modes. Traditional BC pipelines cannot utilize this data. However, UF-OPS can utilize this on-policy data containing both successes and failures.

Our method follows a general four-step framework:

- 1) Train an initial policy $\pi_0(\mathbf{a}|\mathbf{s})$ with behavior cloning to imitate demonstrations of a target task.

- 2) Collect successful and failed trajectories through policy evaluation.
- 3) Train an additional verifier model $C(\mathbf{s}, \mathbf{a}, t)$ that predicts a score, e.g., the success probability of the action, for a given state-action pair at each step of the trajectory.
- 4) Finally, use the verifier prediction to *steer* the policy's action prediction towards a sample with higher score.

This approach combines the strengths of classifier or Q-guided methods like V-GPS—avoiding compute-intensive updates to the policy—with the advantages of online RL approaches—self-improvement instead of relying on data gathered by other policies.

From an RL perspective, this framework can be interpreted as one iteration of a policy improvement scheme [41]. However, in the online, on-policy case with binary rewards, which is the setting we focus on, Q-learning simplifies to success prediction, so we do not require the full overhead of RL to obtain or justify our choice of verifier functions.

A. Data

For our setting, we assume a base diffusion policy $\pi_0(\mathbf{a}|\mathbf{s})$ for a given task. The policy undergoes standard evaluation and a new dataset is collected: $D' = \{\tau_1, \dots, \tau_N\}$ where $\tau_n = (\{\mathbf{s}_0, \mathbf{a}_0, \dots, \mathbf{s}_T, \mathbf{a}_T\}, r_n)$ is the n -th trajectory, \mathbf{s}_i and \mathbf{a}_i are the i -th state and action in the trajectory, respectively, and r_n is the binary success signal of the n -th trajectory., and N is the number of rollouts collected. To avoid complex dense labeling of trajectories, we limit ourselves to the sparse binary signal of final episode success, which is often already collected as part of performance calculation.

B. Implementation

For our experiments, we train the base BC policy using Diffusion Policy [3], but other stochastic policy parameterizations can also be used. For guidance and/or steering to be feasible, we require stochasticity and some level of variance so that generated action samples are adequately different. While Diffusion Policies are initially stochastic, when trained for too long, they tend to become deterministic, producing actions with negligible variance. This would effectively collapse a Best-of-N strategy to a Best-of-1. Especially for single task environments, this can occur rather quickly.

We focus on light-weight verifiers trained with relatively small datasets of rollouts, as collecting many policy failures

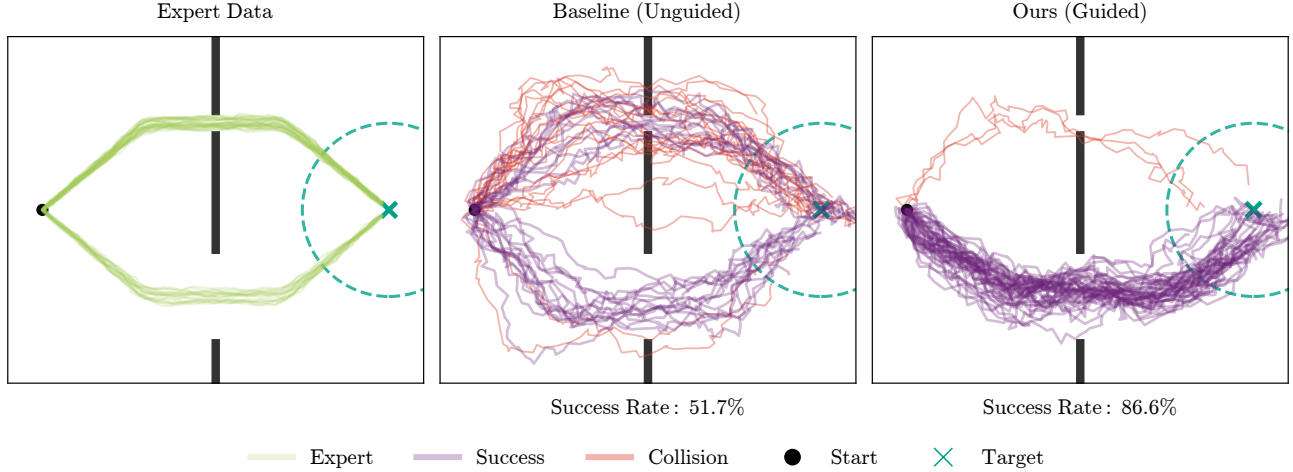


Fig. 4: 2D Toy Example. The expert demonstrations follow S-curves that go through the two doors. The unguided baseline frequently fails at the narrow door. Therefore our guided method redirects traffic favoring the wide door.

can be time-consuming in a real world robot setting. In the binary reward case, the two major options for verifier design are success prediction and time-to-success prediction, which we explore below.

Success Classification with Contrastive Auxiliary Loss. With the labeled trajectory data, we can construct a classifier $C(s, a, t)$ that predicts whether a given state-action pair on a given timestep t within the trajectory belongs to a successful episode or not. We found it helpful to further regularize the representation of the classifier by adding an auxiliary contrastive loss [42]. For this, each positive sample $\mathbf{s}^+, \mathbf{a}^+$ i.e. a transition coming from a successful trajectory, is paired with a negative sample $\mathbf{s}^-, \mathbf{a}^-$ i.e. a transition coming from a failed trajectory at a random timestep, and vice versa. The auxiliary loss is then, a simple distance between the embeddings, shown in Eq. 5.

$$\mathcal{L}_{aux} = \frac{1}{N} \sum_{i=1}^N \left(\max(0, m - \|\mathbf{z}(\mathbf{s}^+, \mathbf{a}^+, t^+) - \mathbf{z}(\mathbf{s}^-, \mathbf{a}^-, t^-)\|_2) \right)^2 \quad (5)$$

where m is a similarity threshold and $z(s, a, t)$ is the penultimate layer of the classifier network. Empirically, we found that adding the episode progress timestep as an input embedding to the classifier network improved performance and helped with disambiguation of state-action pairs with regards to the success label.

To keep our design simple, we used MLPs for our classifier network and a standard sinusoidal embedding [43] for the episode progress timestep t . We provide the equation in Appendix A.

Finally, the full loss used to train the classifier is presented in Eq. 6:

$$\mathcal{L} = \mathcal{L}_{BCE} + \lambda_{aux} \cdot \mathcal{L}_{aux} \quad (6)$$

where \mathcal{L}_{BCE} is a standard Binary Cross Entropy loss and λ is a weight hyperparameter. For our experiments, we used $\lambda_{aux} = 0.1$ and $m = 1.0$.

Time-To-Success Estimation. To obtain a time-to-success predictor, we adapt the common exponential discounting scheme from value function learning in RL. If we interpret the success label as the final and only reward for the trajectory, the Q function at each timestep t is equal to the exponentially discounted time-to-go of the trajectory:

$$Q(\mathbf{s}_t, \mathbf{a}_t, t) = \gamma^{T-t} \cdot r_T, \quad (7)$$

where T is the timestep of success in the trajectory, r_T is the reward on that timestep, and γ is a discount factor. For our experiments, we used $\gamma = 0.99$. Note that for a failed trajectory, the score for each state-action pair is again 0.

We can easily compute this target for each sample in the dataset and fit a function with MSE regression to predict the discounted expected time-to-success. Since we are dealing purely with on-policy data, we can forgo complicated methods such as bootstrapping or off-policy corrections, which greatly simplifies and stabilizes training and the interpretation of the method. Similarly to the classifier, we use simple MLPs as our network choice, and also pass in a sinusoidal embedding of the episode progress timestep t as input to the network.

C. Steering and Guidance Strategies

Given a good verifier function, there are multiple choices for guidance strategies. Below we describe the two variants explored.

Inference-time Action Selection. The simplest way to use a verifier is to generate and rank multiple action candidates. Several related methods for this have been proposed in the literature if the verifier scores are sound [16, 17, 19, 35]. For our experiments, similarly to [35], we adopt the simplest best-of-N strategy with a greedy argmax (Eq. 8).

$$a_{\text{selected}} = \arg \max_{\mathbf{a} \in \mathcal{A}_{\text{prop}}} C(\mathbf{s}, \mathbf{a}, t) \quad (8)$$

We provide pseudo-code for inference-time action selection algorithms in Algorithm 1.

Algorithm 1 Verifier Best-of-N Steering

Require: Policy $\pi_0(s, a)$, verifier function $C(s, a, t)$, number of action samples N , max steps T for a rollout

- 1: Initialize $t \leftarrow 0, s_0$
- 2: **for** $t = 0$ to T **do**
- 3: Sample $\{\mathbf{a}_{t_0}, \mathbf{a}_{t_1}, \dots, \mathbf{a}_{t_{N-1}}\}$ from π_0
- 4: $\mathcal{A}_t \leftarrow \{\mathbf{a}_{t_0}, \dots, \mathbf{a}_{t_{N-1}}\}$
- 5: $\mathbf{a}_t \leftarrow \operatorname{argmax}_{\mathbf{a} \in \mathcal{A}_t} C(s_t, \mathbf{a}, t)$
- 6: **end for**

Classifier Guidance. Instead of optimal action selection among a number of candidates, we can perturb the generated action using the verifier as an energy-based model [44]. The most common framework in the context of diffusion models is classifier-guided sampling or more generally, objective-guided sampling, similarly to [45]. We, thus, adapt the traditional classifier guidance approach within the DDPM [39] framework.

Standard classifier guidance would require training the verifier to distinguish actions at all noise levels. In practice, we did experiment with training a classifier on state, trajectory progress timestep, and a noisy action chunk on a random timestep of the diffusion process, calculated using the forward chain of the base policy noise scheduler. However, this caused our verifiers to ignore the action and predict success and failure based solely on the state, which constitutes the verifier unsuitable for this task. We are thus limited to verifier functions trained only on unmodified observation-action pairs as obtained by the rollouts.

To apply classifier guidance using the classifier trained only on the fully denoised actions, we apply the modification for DDPM proposed by Bansal et al. [46]. Standard classifier guidance applies the gradient of the classifier on the one step denoised sample at every iteration of the reverse diffusion process. In this modified version, the classifier forward pass is done using the mean prediction of the final clean sample $\hat{\mathbf{a}}_0$ which DDPM approximates at every step of the reverse process. The gradient of the classifier w.r.t. $\hat{\mathbf{a}}_0$, $\lambda \nabla_{\hat{\mathbf{a}}_0} C(s, \hat{\mathbf{a}}_0, t)$ is then multiplied by a strength guidance λ and added as perturbation to $\hat{\mathbf{a}}_0$ and the remainder of the denoising step uses the new perturbed mean $\hat{\mathbf{a}}_0$. We include the DDPM modification in the context of our method in Algorithm 2.

D. Pedagogical Navigation Task

To build intuition for the kinds of failures test-time adaptation can address, we consider a simple 2D navigation task. The goal of this task is to go from the start point (left) to the green goal circle on the right without colliding with a wall (Fig. 4). The agent can control the velocity towards the next waypoint from any given x,y coordinate. Any path must pass through one of two doors, a wide or a narrow one. Using the wide door is easier as the trajectory does not have to be as precise.

The expert data used to train the base diffusion policy are constructed from successful trajectories traversing either of the two doors at equal proportion. We expect the trained diffusion policy to fail to produce precise enough trajectories to achieve high performance in this task. Evaluating the resulting diffu-

Algorithm 2 Verifier Classifier-Guidance with DDPM

Require: Diffusion policy $\pi_0(s, a)$ trained as a noise predictor ϵ_θ , verifier function $C(s, a, t)$, gradient scale s , guidance strength λ , max steps T for a rollout, K diffusion steps.

- 1: Initialize $t \leftarrow 0, s_0$ initial sim/real state.
- 2: Initialize noise schedule parameters $\alpha_k, \bar{\alpha}_k, \sigma_k^2$ for $k = 1 \dots K$.
- 3: **for** t from 0 to T **do**
- 4: Sample $\mathbf{a}_K^0 \sim \mathcal{N}(\mathbf{0}, \mathbf{I})$
- 5: **for** k from K down to 1 **do**
- 6: $\mathbf{z} \sim \mathcal{N}(\mathbf{0}, \mathbf{I})$ if $k > 1$, else $\mathbf{z} = \mathbf{0}$
- 7: $\epsilon \leftarrow \epsilon_\theta(s_t, \mathbf{a}_k^t, k)$
- 8: $\hat{\mathbf{a}}_0^t \leftarrow \frac{1}{\sqrt{\bar{\alpha}_k}} \left(\mathbf{a}_k^t - \frac{\sqrt{1-\bar{\alpha}_k}}{\sqrt{1-\bar{\alpha}_k}} \epsilon \right)$
- 9: $\hat{\mathbf{a}}_0^t \leftarrow \hat{\mathbf{a}}_0^t + \lambda \nabla_{\hat{\mathbf{a}}_0} \log C(s_t, \hat{\mathbf{a}}_0^t, t)$
- 10: $\tilde{\mu}_k \leftarrow \frac{\sqrt{\bar{\alpha}_{k-1}} \beta_k}{1-\bar{\alpha}_k} \mathbf{a}_k^t + \frac{\sqrt{\bar{\alpha}_k(1-\bar{\alpha}_{k-1})}}{1-\bar{\alpha}_k} \hat{\mathbf{a}}_0^t$
- 11: $\mathbf{a}_{k-1}^t \leftarrow \tilde{\mu}_k + \sigma_k^2 \cdot s \cdot + \sigma_k \mathbf{z}$
- 12: **end for**
- 13: **end for**
- 14: **return** \mathbf{a}_0^t

sion policy on 1000 rollouts confirms our expectation with a success rate of 52%. The majority of failures, shown in Fig. 4 result from the failure to navigate the narrow door.

The evaluation trajectories are subsequently used to train a simple MLP classifier. The classifier is used during rollout in a Best-of-N fashion to select the highest scoring of 30 candidates sampled from the base policy. The steered policy is evaluated on 1000 rollouts and yields a success rate of 85.1%. Expert demos and samples of generated trajectories from the unguided and guided policies respectively, are presented in Fig. 4.

In addition, we provide a visualization of the learned classifier landscape to showcase its preference at the start of a trajectory, in Fig. 5. This demonstrates that already from the very beginning of a rollout, the classifier scores transitions that belong to the distribution mode corresponding to the wide door more highly. As a result, the guided policy is skewed to prefer the wide door. It is also notable that the generated trajectories from the guided policy form much tighter clusters and that seems to be the case for both distribution modes corresponding to the two doors. That increases the chance of success even for the narrow door.

V. EXPERIMENTS

Our experimental setup is comprised of 4 simulation tasks from the Robomimic suite [6], namely low dimensional state Transport and Square, and image based Transport and Square. Transport involves bimanual handing over of a hammer, and Square requires performing insertion of a square prop into a peg. Our real experiments include 5 manipulation tasks on the Aloha system [12]. For low dimensional state, the observation is used as is as input to the verifier function while for image based policies, we use the frozen embedding from the vision encoder of the base policy.

TABLE I: Performance (%) on Robomimic SIM tasks: Comparison of the base policy against 4 combinations of our method, Q function with Best-of-N (Q x BoN), classifier with Best-of-N (C x BoN), Q function with classifier guidance (Q x CG) and classifier with classifier guidance (C x CG). The method is also compared against 2 baselines, SAILOR [47], and DSRL [36].

Task	Base	SAILOR [47]	DSRL [36]	Q x BoN	C x BoN	Q x CG	C x CG
Transport (low dim)	56.6 ± 3.07	-	24.8±9.0	59.6±3.04	60.7±3.03	66.9±2.92	64.7±3.0
Square (low dim)	78.2 ± 2.56	-	74±6.1	85.1±2.2	86.0±2.2	81.7±2.4	85.5±2.2
Transport (image)	58.1 ± 3.06	5.9 ± 1.46	-	65.7 ± 2.94	71.9 ± 2.79	62.5 ± 3.0	60.7 ± 3.03
Square (image)	70.1 ± 2.84	45.1 ± 3.08	-	75.9±2.7	83.5±2.3	76.4±2.63	77.6±2.6

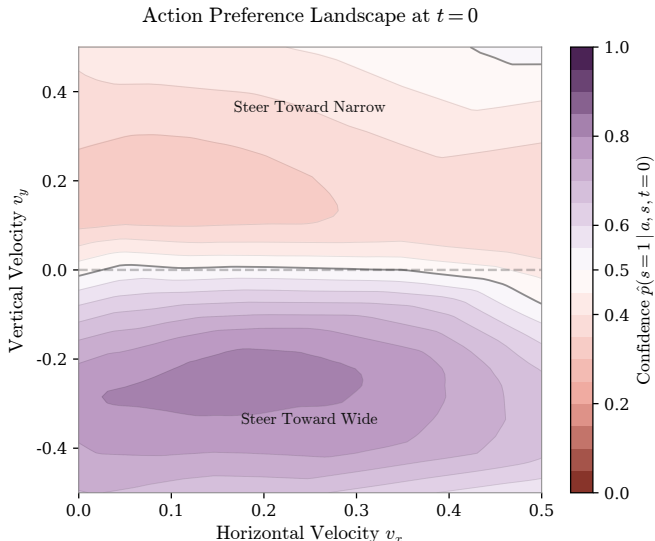


Fig. 5: 2D Toy Example. The classifier correctly identifies the wide door (purple region) as the safer option.

A. Simulation Results

For our simulation experiments, we pretrain a set of base diffusion policies for the 4 simulation environments using the absolute action multi-human (MH) Robomimic datasets [6]. Each of the Robomimic MH datasets contains 300 demonstrations from 6 human operators of varying proficiency. As the diffusion policy model, we use the default U-Net [48] with a ResNet18 [49] backbone configuration for Robomimic environments, provided with [3]. The noising and denoising is controlled by a DDPM [39] scheduler with 100 diffusion training and inference timesteps. The policy takes in the two Robomimic camera images, top down and agent view, along with proprioception as the current observation, and another same dimension input as one historical context. The output is an action chunk of 8. At evaluation, each transition contains an action chunk of 8 and current plus one historical observation since this is the input and output of the policy. More details on these datasets can be found in Appendix A. To prevent training to the point of deterministic predictions and preserve the variance necessary for steering, we train the low dimensional policies for 350 epochs and the image based policies for 150 epochs. We collect 6048 trajectories for the low dimensional environments and 12012 trajectories for the image environments. Low dimensional square trajectories contain 50 steps, low dimensional transport trajectories contain 88 steps, and

both image square and image transport trajectories contain 63 steps. We use as episode success label the binary signal from the simulator.

Subsequently, the episode label is propagated at every step of a trajectory in the case of the classifier, or each transition is annotated with its discounted expected return in the case of the time-to-success estimation. Note that both can easily be done on the fly at verifier training time. Trajectories - not transitions - are split 80-20 between training and validation, to prevent validation set contamination. Verifiers are trained for 200 epochs and the checkpoint with the lowest validation loss is chosen for guidance. For classifier guidance, in practice we apply the gradient of the time-to-success Q estimation intact but still take the log of the classifier. For steering with Best-of-N argmax, $N = 10$ suffices. For classifier guidance, we present results for the best guidance strength per task. Specific architectures and hyperparameters can be found in Appendix A.

We compare our results against two recent works, DSRL [36] and SAILOR [47]. In DSRL, RL is used to steer the initial latent diffusion noise to select different behavioral sequences. SAILOR employs a world and reward model to learn recovery strategies post-training. To provide a fair comparison, we limit all methods to the same number of on-policy interactions as used for our verifier training. Tab. I shows that our method surpasses DSRL and SAILOR for the same number of on-policy interactions. For an expanded discussion of base policy performance, see Appendix B.

B. Real experiments

To evaluate our method beyond simulation, we construct 5 real tasks on the Aloha bimanual system [12]. More specifically, we set up the following tasks: a) pick up the block and place it on the cardboard, b) pick up the ball and place it in the bowl, c) pick up the hammer with the right hand, hand it over to the left and drop it in the box, real counterpart to Robomimic Transport, d) pick up the pen cap with the right hand and the cap with the left and insert it on the pen, and e) pick up the green cup and stack it on the purple. Our setup can be seen in Fig. 3.

For each task, we collect 100 demonstrations. We train each base policy for 80000 steps with an action chunk of 8 and current observation only. Similarly to simulated experiments, the base policy model is an image-based U-Net [48] with a ResNet18 [49] backbone. In contrast to simulation, we use a DDIM [40] noise scheduler with 50 diffusion training and

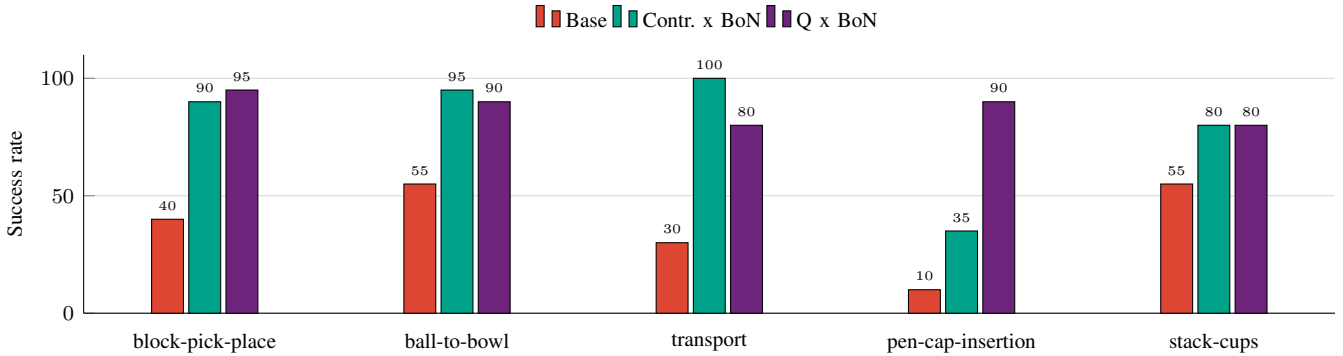


Fig. 6: Performance comparison on 5 real Aloha tasks: block pick and place, ball to bowl, transport, pen cap insertion and cup stacking. Steering using a verifier function boosts performance of the base policy performance for all 5 tasks significantly.

inference timesteps. The base policy uses the 3 out of the 4 cameras of the Aloha system as observation - top down, left wrist, right wrist - as well as the proprioceptive joint state. During evaluation, we set 750 max steps for the rollouts for all tasks except pen cap insertion, which is more long-horizon, where we increased the max steps to 1300. Each policy is evaluated and 60 rollouts are saved for training verifier functions. For each task, we train a Q function and a classifier, similarly to our simulation experiments. The rollouts are saved along with a binary, user inputted success label. We train the Q function for 200 epochs and the classifier for 400 epochs and select the checkpoint with the best validation loss per verifier type.

We then perform 20 trials for each task, for the base and for each verifier function respectively. For our real experiments, we choose Best-of-N with $N = 10$ as our steering mechanism, for its ease and simplicity. Results are presented in Fig. 6. As seen, steering with a verifier function increases performance of the base policy on all instances, with gains spanning from 25% to 80%. It is worth noting that the Q function and classifier are both on par for most tasks except pen cap insertion. For this task, while the classifier still boosts performance, the increase does not compete with that of the Q function steering. We hypothesize that the difference lies in the fact that pen cap insertion is distinctly more long-horizon than the other 4 tasks. Thus, the Q function trained with time-to-success estimation is possibly a better scorer for such long-horizon tasks.

C. On-policy vs off-policy rollouts

Inspired by [35], we seek to answer the question of how important *on-policy* data is for the efficacy of our method. We thus, conduct a set of experiments that leverage rollouts of one policy to steer a different base policy. More specifically, we trained a second set of base diffusion policies for low dimensional Transport and Square. For these, we use the absolute action proficient human (PH) Robomimic datasets [6]. For fairness, we keep all the parameters of the base policy and verifier training the same.

Subsequently, we choose the simple Best-of-N steering strategy and attempt to guide the MH policy using the verifiers derived from rollouts from the PH policy and vice versa. As expected, the base PH policies perform better than their MH

counterparts given they are trained on fewer but higher quality demonstrations. Therefore, the verifiers trained on rollouts from PH versus MH are off-policy with respect to one another. Ablation results are presented in Tab. II.

TABLE II: Comparison of steering via verifiers trained on off-policy, yet task related, data reveals that leveraging on-policy rollouts is crucial for the efficacy of the method.

Task	Base	Q x BoN	C x BoN
PH \rightarrow MH Transport (low dim)	56.6 \pm 3.07	54.7 \pm 3.09	54.3 \pm 3.09
PH \rightarrow MH Square (low dim)	78.2 \pm 2.56	78.6 \pm 2.54	79.8 \pm 2.49
MH \rightarrow PH Transport (low dim)	81.1 \pm 2.43	79.5 \pm 2.5	79.4 \pm 2.51
MH \rightarrow PH Square (low dim)	90.7 \pm 1.8	90.7 \pm 1.8	93.7 \pm 1.51

We conclude that on-policy rollouts for verifier training and steering play a critical role in the success of the method. Training a verifier on rollouts from a better policy (PH) and using it to steer a policy derived from noisier data does not improve success rates and sometimes even regresses performance. Similarly, training a verifier on rollouts from a policy derived from noisier data and using it to steer a policy trained on cleaner data also fails to boost performance. This highlights how offline data collected from other policies are not suitable for improving policy performance via inference-time steering.

VI. LIMITATIONS

Although this work presents a general framework for improving the performance of a base policy using existing evaluation data that would otherwise typically be unused, there are some noteworthy limitations. Firstly, we only examined single task policies with different verifier-sampling recipes working best for different tasks. It is very possible that continuing this work on multi-task policies could unlock new insights and new design choices for suitable verifiers. Secondly, applying this work to real still maintains a small overhead of manual labeling of successful and failed rollouts. Finally, specifically classifier guidance as a method of steering is proven to be very sensitive to guidance strength which is a free hyperparameter tunable on a per task level. In addition, tuning this in real

potentially poses some safety risks. Despite these limitations, we believe this is an exciting direction for further research.

VII. CONCLUSION

In this work, we presented a framework for policy improvement solely at test-time without tedious fine-tuning or expensive data collection requirements. Our approach relied on the policy’s own experience i.e. its own successful and failed rollouts, to train a guidance model, namely a verifier function. At sampling time, the verifier function was optimized in order to select better action samples or refine predicted samples using its gradient. Ultimately, we showed that obtaining a good verifier leads to a consistent, low cost performance improvement.

ACKNOWLEDGMENTS

The authors would like to thank Dhruv Shah, Dushyant Rao, Florian Shkurti, Jonathan Kelly, and Jonathan Tompson for fruitful discussions and helpful feedback. Finally, the authors would like to extend a special thanks to Vikas Sindhwani and Carolina Parada for their continued support without which this work would not have been possible.

APPENDIX A IMPLEMENTATION DETAILS

A. Low dimensional experiments

1) *Model architecture*: The architecture used for the Q function of the low dimensional experiments is comprised by two 2 linear layer followed by ReLU encoders, one for observation and one for action, along with a sinusoidal embedding for the timestep of the transition within the episode. Those embeddings are concatenated and passed through an MLP containing 2 blocks of linear layer, layernorm, ReLU followed by a 0.5 dropout and a final linear layer. For the contrastive classifier, the architecture is identical however the output of the last ReLU and before the dropout is used as the contrastive embedding and the final linear layer as the classification head.

The sinusoidal embedding used is described by:

$$\text{Emb}(t, j) = \begin{cases} \sin\left(\frac{t}{10000^{\frac{j}{d}}}\right) & \text{if } j \text{ is even,} \\ \cos\left(\frac{t}{10000^{\frac{j-1}{d}}}\right) & \text{if } j \text{ is odd.} \end{cases} \quad (9)$$

Finally, for all low dimensional experiments, we used a time embedding dimension, encoder dimension and second hidden dimension of 64 as well as a first hidden dimension of 128.

2) *Classifier guidance strength*: For the low dimensional environments, we used classifier guidance strength of $\lambda = 0.1$ for classifier experiments and $\lambda = 0.5$ for time-to-success experiments.

B. Image experiments

1) *Model architecture*: The architecture used for the Q function of the image based experiments is comprised by 2 encoders, one for observation and one for action. Each encoder has a spectral norm applied on a linear layer followed by a layernorm, GELU, another spectral norm over a linear

layer and a layernorm. The observation is first passed by a layernorm and noise augmentation with std 0.02 at training time only, is added. Then the observation and action are passed by the respective encoders. The results are concatenated along with the sinusoidal embedding of the episode timestep of the transition and this input is passed through an MLP containing 2 blocks of a spectral norm over a linear layer, layernorm, ReLU with a 0.1 dropout in between, followed by a final linear layer. The contrastive classifier has the same architecture with the only difference being that a 0.5 dropout is used and the dropout along with the final linear layer play the role of the classifier head, where the output of the layers before the dropout serve as the embedding.

For all image experiments including real but excluding transport image, we used a time embedding dimension of 128, an encoder dimension and second hidden dimension of 256 and a first hidden dimension of 512. For transport image, we used the same dimensions as the low dimensional experiments.

2) *Classifier guidance strength*: For the image environments, we used classifier guidance strength of $\lambda = 0.1$ for the classifier and $\lambda = 0.5$ for the time-to-success model for Square Image, while we used $\lambda = 0.05$ for the classifier and $\lambda = 0.8$ for the time-to-success model for Transport Image. This seems to indicate that image based environments are more sensitive to guidance strength which unfortunately is a limitation of this steering strategy.

APPENDIX B DISCUSSION OF BASELINE COMPARISON

Curiously, we find that both methods underperform a well-trained diffusion policy baseline on some tasks. This is explained by the fact that both methods are built for significantly longer training with more on-policy samples. Especially for DSRL, training for longer and with more samples does eventually lead to strong performance, as reported by Wagenmaker et al. [36]. Interestingly, while DSRL starts with a similar baseline performance as our policy, training first decreases the performance as the RL components struggle to fit their targets with limited data, and only starts surpassing the baseline on transport after an order of magnitude more samples than used here. In addition, DSRL requires a diffusion model with significantly fewer denoising steps to make efficient training possible. This further decreases performance of the underlying model, whereas our method is able to work with an expensive and capable DP base.

In addition, the training of DSRL and SAILOR is significantly slower than our method. For comparison, collecting 6000 trajectories for the square task takes circa two and a half hours on a RTX3090 GPU, with the runtime mostly dominated by the diffusion model prediction. Fully training DSRL for the same number of steps takes an additional 4 hours, while training our verifier functions only takes about 20 minutes.

APPENDIX C ALOHA REAL SPECIFICATIONS AND BASE POLICIES

For the real setup, we used the standard Aloha stationary system provided by Trossen Robotics. The Aloha real setup

is comprised by two ViperX follower arms that perform the tasks, and two WidowX leader arms used for puppeteering for data collection. The setup also has 4 RealSense D405 cameras, one center overhead, one worms eye at the center of the table, and two wrist cameras mounted on the follower arms. Our installation follows the standard Trossen documentation and scripts. However, for data collection, we opted to amend the Trossen provided scripts to allow for variable episode length.

REFERENCES

- [1] A. Brohan *et al.*, “Rt-1: Robotics transformer for real-world control at scale,” in *Robotics: Science and Systems (RSS)*, 2023.
- [2] A. Brohan *et al.*, “Rt-2: Vision-language-action models transfer web knowledge to robotic control,” in *Conference on robot learning (CoRL)*, 2023.
- [3] C. Chi *et al.*, “Diffusion policy: Visuomotor policy learning via action diffusion,” in *Robotics: Science and Systems (RSS)*, 2023.
- [4] K. Black *et al.*, “ π_0 : A vision-language-action flow model for general robot control,” *arXiv preprint arXiv:2410.24164*, 2024.
- [5] M. J. Kim *et al.*, “Openvla: An open-source vision-language-action model,” in *Conference on Robot Learning*, 2025.
- [6] A. Mandlekar *et al.*, “What matters in learning from offline human demonstrations for robot manipulation,” in *Neural Information Processing Systems (NeurIPS)*, 2021.
- [7] S. Ross *et al.*, “A reduction of imitation learning and structured prediction to no-regret online learning,” in *International Conference on Artificial Intelligence and Statistics (AISTATS)*, 2011.
- [8] C. Wen *et al.*, “Fighting copycat agents in behavioral cloning from observation histories,” *Neural Information Processing Systems (NeurIPS)*, 2020.
- [9] P. Florence *et al.*, “Implicit behavioral cloning,” in *Conference on Robot Learning (CoRL)*, 2022.
- [10] A. Mandlekar *et al.*, “Human-in-the-loop imitation learning using remote teleoperation,” *arXiv preprint arXiv:2012.06733*, 2020.
- [11] N. M. Shafullah *et al.*, “Behavior transformers: Cloning k modes with one stone,” *Neural Information Processing Systems (NeurIPS)*, 2022.
- [12] T. Z. Zhao *et al.*, “Learning fine-grained bimanual manipulation with low-cost hardware,” in *Robotics: Science and Systems (RSS)*, 2023.
- [13] S. Belkhal *et al.*, “Data quality in imitation learning,” *Neural Information Processing Systems (NeurIPS)*, 2023.
- [14] M. Kelly *et al.*, “Hg-dagger: Interactive imitation learning with human experts,” in *IEEE/RSJ International Conference on Robotics and Automation (ICRA)*, 2019.
- [15] M. Laskey *et al.*, “Dart: Noise injection for robust imitation learning,” in *Conference on Robot Learning (CoRL)*, 2017.
- [16] N. Ma *et al.*, “Inference-time scaling for diffusion models beyond scaling denoising steps,” *arXiv preprint arXiv:2501.09732*, 2025.
- [17] X. Zhang *et al.*, “Inference-time scaling of diffusion models through classical search,” in *International Conference on Learning Representations (ICLR)*, 2026.
- [18] M. Du and S. Song, “Dynaguide: Steering diffusion policies with active dynamic guidance,” in *Neural Information Processing Systems (NeurIPS)*, 2025.
- [19] Y. Wang *et al.*, “Inference-time policy steering through human interactions,” in *IEEE International Conference on Robotics and Automation (ICRA)*, 2025.
- [20] Y. Wu *et al.*, “From foresight to forethought: Vlm-in-the-loop policy steering via latent alignment,” in *Robotics: Science and Systems (RSS)*, 2025.
- [21] M. Wolczyk *et al.*, “Fine-tuning reinforcement learning models is secretly a forgetting mitigation problem,” in *International Conference on Machine Learning (ICML)*, 2024.
- [22] K. Bousmalis *et al.*, “Robocat: A self-improving generalist agent for robotic manipulation,” in *International Conference on Learning Representations (ICLR)*, 2025.
- [23] Y. Jin *et al.*, “Sime: Enhancing policy self-improvement with modal-level exploration,” in *IEEE/RSJ International Conference on Intelligent Robots and Systems (IROS)*, 2025.
- [24] Y. Jin *et al.*, “Soe: Sample-efficient robot policy self-improvement via on-manifold exploration,” in *IEEE International Conference on Robotics and Automation (ICRA)*, 2026.
- [25] N. Hirose *et al.*, “Selfi: Autonomous self-improvement with reinforcement learning for social navigation,” in *Conference on Robot Learning (CoRL)*, 2024.
- [26] A. Nair *et al.*, “Awac: Accelerating online reinforcement learning with offline datasets,” in *Deep Reinforcement Learning Workshop, Neural Information Processing Systems (NeurIPS)*, 2020.
- [27] S. K. S. Ghasemipour *et al.*, “Self-improving embodied foundation models,” in *Neural Information Processing Systems (NeurIPS)*, 2025.
- [28] M. A. Raad *et al.*, “Scaling instructable agents across many simulated worlds,” *arXiv preprint arXiv:2404.10179*, 2024.
- [29] M. Jia *et al.*, “Seil: Simulation-augmented equivariant imitation learning,” in *IEEE International Conference on Robotics and Automation (ICRA)*, 2023.
- [30] H. Oh *et al.*, “Self-augmented robot trajectory: Efficient imitation learning via safe self-augmentation with demonstrator-annotated precision,” *arXiv preprint arXiv:2509.09893*, 2025.
- [31] A. S. Chen *et al.*, “Curating demonstrations using online experience,” in *Robotics: Science and Systems (RSS)*, 2026.
- [32] A. Ajay *et al.*, “Is conditional generative modeling all you need for decision-making?” in *Neural Information Processing Systems (NeurIPS)*, 2022.
- [33] K. Frans *et al.*, “Diffusion guidance is a controllable policy improvement operator,” *arXiv preprint arXiv:2505.23458*, 2025.
- [34] Y. Liu *et al.*, “Bidirectional decoding: Improving action chunking via guided test-time sampling,” in *International Conference on Learning Representations (ICLR)*, 2025.
- [35] M. Nakamoto *et al.*, “Steering your generalists: Improving robotic foundation models via value guidance,” in *Conference on Robot Learning (CoRL)*, 2024.
- [36] A. Wagenmaker *et al.*, “Steering your diffusion policy with latent space reinforcement learning,” in *Conference on Robot Learning (CoRL)*, 2025.
- [37] F. Torabi *et al.*, “Behavioral cloning from observation,” in *International Joint Conference on Artificial Intelligence (IJCAI)*, 2018.
- [38] P. Dhariwal and A. Nichol, “Diffusion models beat gans on image synthesis,” *Neural Information Processing Systems (NeurIPS)*, 2021.
- [39] J. Ho *et al.*, “Denoising diffusion probabilistic models,” in *Neural Information Processing Systems (NeurIPS)*, 2020.
- [40] J. Song *et al.*, “Denoising diffusion implicit models,” in *International Conference on Learning Representations (ICLR)*, 2021.
- [41] R. S. Sutton and A. G. Barto, *Reinforcement Learning: An Introduction*. MIT Press, 1998.
- [42] R. Hadsell *et al.*, “Dimensionality reduction by learning an invariant mapping,” in *IEEE Computer Society Conference on Computer Vision and Pattern Recognition (CVPR)*, 2006.
- [43] A. Vaswani *et al.*, “Attention is all you need,” *Neural Information Processing Systems (NeurIPS)*, 2017.
- [44] Y. Du and I. Mordatch, “Implicit generation and generalization in energy-based models,” in *Neural Information Processing Systems (NeurIPS)*, 2019.
- [45] M. Janner *et al.*, “Planning with diffusion for flexible behavior synthesis,” in *International Conference on Machine Learning (ICML)*, 2022.
- [46] A. Bansal *et al.*, “Universal guidance for diffusion models,” in *the IEEE/CVF conference on computer vision and pattern recognition*, 2023.
- [47] A. K. Jain *et al.*, “A smooth sea never made a skilled SAILOR: Robust imitation via learning to search,” in *Neural Information Processing Systems (NeurIPS)*, 2025.
- [48] O. Ronneberger *et al.*, “U-net: Convolutional networks for biomedical image segmentation,” in *Medical Image Computing and Computer-Assisted Intervention (MICCAI)*, 2015.
- [49] K. He *et al.*, “Deep residual learning for image recognition,” in *IEEE Computer Society Conference on Computer Vision and Pattern Recognition (CVPR)*, 2016.